ELSEVIER

Contents lists available at ScienceDirect

## Sensors and Actuators: A. Physical

journal homepage: www.journals.elsevier.com/sensors-and-actuators-a-physical



# Smartphone-based optical fiber sensor for refractive index sensing using POF

Muhammad Saleh Urf Kumail Haider <sup>a,1</sup>, Chen Chen <sup>a,\*,2</sup>, Abdul Ghaffar <sup>b</sup>, Laraib Unsa Noor <sup>c</sup>, Min Liu <sup>a</sup>, Sadam Hussain <sup>b,3</sup>, Bipu Arman <sup>d</sup>, Moath Alathbah <sup>e</sup>

- <sup>a</sup> School of Microelectronics and Communication Engineering, Chongqing University, Chongqing 400044, China
- b Key Laboratory of Air-Driven Equipment Technology of Zhejiang Province, College of Mechanical Engineering, Quzhou University, Quzhou, Zhejiang 32400, China
- College of Mechanical and Vehicle Engineering, Chongqing University, Chongqing 400044, China
- <sup>d</sup> College of Optoelectronic Engineering, Chongqing University, Chongqing 400044, China
- <sup>e</sup> Department of Electrical Engineering, College of Engineering, King Saud University, Riyadh 11451, Saudi Arabia

#### ARTICLE INFO

#### Keywords: Coupling Portable sensor Plastic optical fiber (POF) Refractive index (R.I.)

#### ABSTRACT

This paper presents a portable optical fiber sensor (OFS) for refractive index (R.I.) sensing, fabricated using two pieces of bare polymer optical fibers (POFs). The proposed sensor design utilizes the twisted macro-bending and optical coupling (TMBOC) technique, where two optical fibers are twisted and coupled, leading to power coupling from the primary fiber (PF) to the coupled fiber (CF). A 3D-printed smartphone casing is used to attach the sensor with a smartphone, connecting the fibers to the flashlight and camera. The R.I. sensing relies on the power loss coupling phenomenon, in which light travels to the PF and the CF couples the power, resulting in intensity variations as the surrounding R.I. medium changes. The proposed R.I. sensor with an 8-mm radius exhibits the maximum sensitivity with different NaCl concentration liquids, with an R.I. range of 1.333–1.361 and a sensitivity of  $137.2 \pm 2.3 \,\%$ /RIU. The experimental findings indicate the sensor's excellent stability and reliability. The sensor's straightforward, comprehensive, and cost-effective design enables its application in chemical, petroleum, biomedical, and other industries.

## 1. Introduction

The refractive index (R.I.) represents a fundamental optical parameter of significant importance across diverse scientific and technological domains. Indirect quantification of physical variables, such as temperature, pressure, and concentration, can be effectively achieved through the detection of variations in the R.I. [1]. Traditional methodologies for measuring the R.I. often involve cumbersome and costly apparatus, which can limit their practical utility and widespread adoption [2]. In contrast, optical fiber sensors (OFSs) have garnered considerable attention due to their inherent advantages over conventional electrical sensors [3]. These benefits include immunity to electromagnetic interference, compactness, and the capability for remote sensing [4]. The portable and cost-effective OFS sensors have grown significantly in

recent years [5,6], driven by the need for real-time monitoring in a variety of fields, including environmental science [7], medical diagnostics [8], and industrial process control [9].

The OFSs for R.I. sensing can be categorized into distinct classes based on their underlying measurement principles. Notable examples include Fabry-Pérot interferometers (FPIs) [10,11], multimode interferometers (MMIs) [12,13], and Mach-Zehnder interferometers (MZIs) [14,15]. Additionally, long-period gratings (LPGs) [16,17] and fiber Bragg gratings (FBGs) [18,19] utilize wavelength modulation, where the R.I. changes induce shifts in the wavelength of the transmitted light [20]. This wavelength modulation approach is generally more sophisticated and necessitates advanced measurement equipment for precise detection [21,22]. In contrast, intensity modulation-based sensors, which rely on changes in light intensity as the R.I. varies [23], offer

E-mail addresses: kumailsandano@gmail.com (M.S.U.K. Haider), c.chen@cqu.edu.cn (C. Chen), ghaffar@qzc.edu.cn (A. Ghaffar), laraibunsanoor@gmail.com (L.U. Noor), liumin@cqu.edu.cn (M. Liu), sadamhussain@qzc.edu.cn (S. Hussain), bipuarman@gmail.com (B. Arman), malathbah@ksu.edu.sa (M. Alathbah).

<sup>\*</sup> Corresponding author.

<sup>&</sup>lt;sup>1</sup> Orcid id 0009–0007-5561–7277

 $<sup>^{2}</sup>$  Orcid id 0000–0003-2541–6283

 $<sup>^3</sup>$  Orcid id 0000–0003-1990–7676

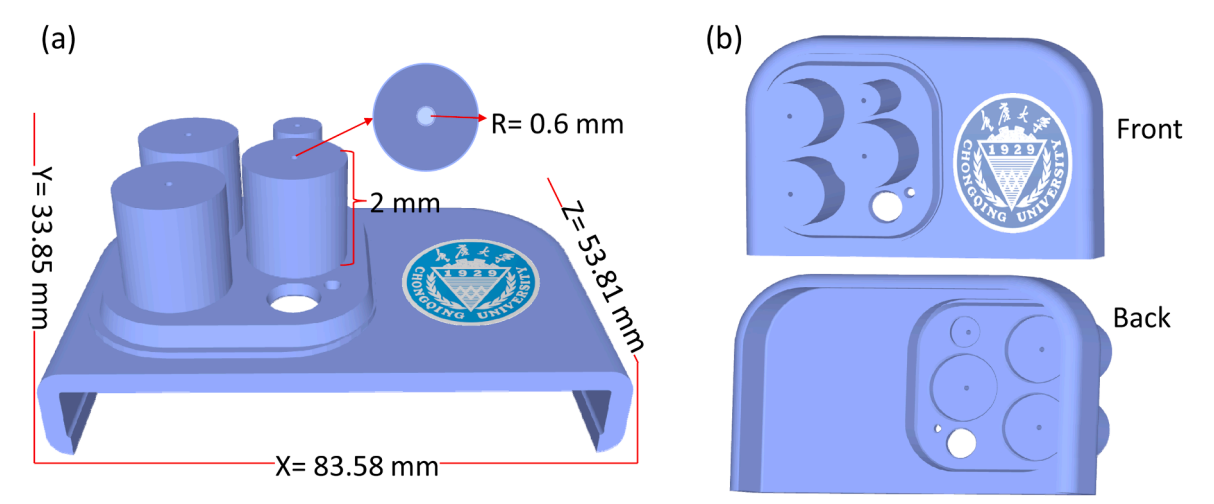


Fig. 1. Design of 3D-printed casing for the proposed R.I. sensor: (a) shows the 3D view of the casing, showcasing the precise dimensions to connect the optical fibers with the smartphone; (b) illustrates the front and back view of the casing.

simpler implementation and straightforward measurement techniques [24,25]. Among intensity modulation-based sensors, polymer optical fibers (POFs) emerge as a cost-effective option, combining affordability with the inherent benefits of optical fibers, such as flexibility and ease of integration with devices like smartphones for portable, real-time R.I. sensing. The demand for POF based R.I. sensors is increased on both intensity and wavelength modulation. The integration of tilted-FBG into POFs has been explored to enhance R.I. sensing capabilities. Hu et al. [26] successfully inscribed tilted-FBGs in step-index POFs, demonstrating their potential for R.I. sensing applications. This work laid the foundation for subsequent research into tilted-FBG-based R.I. sensors utilizing POFs.

Ujihara et al. [27] proposed a tapered graded index per fluorinated POF by employing intense illumination propagation inside fiber to create a R.I. sensor. Similarly, De-Jun et al. [28] utilized the tapered technique for R.I. sensing. These sensors rely on the principle that the evanescent wave generated by propagating light interacts with the surrounding medium, leading to a reduction in optical transmission. A different approach was taken by the authors, who fabricated a D-shaped POF sensor using a side-half-polishing method [29], which also operates based on the interaction between the evanescent wave and the external environment. Yanjun Hu et al. [30] introduced a narrow groove and gold-plated structure-based R.I. sensor, but the fabrication process involved in creating these structures adds complexity and cost to the sensor. Another approach is presented by Shin J.D. et al. [31] and Ye et al. [32], who explored drilling holes in POFs to develop R.I. sensors, including a portable multi-hole sensor. However, the drilling step introduces additional complexity and potential limitations in the sensor's performance. Another study [33] investigated a multiparameter sensor for liquid level and R.I. measurement, using both a notched POF and a U-shaped sensor structure. However, there remains a significant research gap for a simple, cost-effective, and portable R.I. sensor that does not require complex fabrication processes such as drilling or polishing.

Integrating POF sensors with smartphone simplifies their equipment needs, making it a viable and efficient solution. Recent advancements in smartphone technology have led to their integration with various scientific applications due to their enhanced computational power and optical imaging capabilities [34,35]. Smartphones offer a compact, accessible platform, making them ideal for developing portable sensing systems. The smartphone's flashlight can serve as the light source, while the camera functions as the detector, eliminating the need for external LEDs or photodetectors. For example, Malone et al. [36] presented smartphone-based optical coherence tomography systems, leverage smartphone built-in components for detecting, processing, and

displaying data, demonstrating potential for use in low-resource environments. Similarly, Kuang at al. [37] proposed the integration of POF sensors into smartphones for the purpose of monitoring human physiological parameters, including heart and respiratory rates using intensity modulation.

In this paper, we propose a smartphone-based portable R.I. sensor utilizing the commercially available POF, which stands out as a particularly promising solution for portability and affordability. We design a 3D-printed smartphone casing for OFS and attach it to a smartphone to facilitate R.I. sensing. Two bare fibers, twisted macro-bended and optically coupled (TMBOC), are directly integrated with a smartphone for R. I. sensing. One fiber serves as a light source for the smartphone's flashlight, while the other fiber integrates with the smartphone's camera to detect variations in light intensity due to changes in the surrounding medium. Compared to other existing approaches, it provides a simple, cost-effective, and robust method for R.I. sensing. The integration with a smartphone not only ensures simple deployment but also enables seamless data transmission and storage, making it ideal for both laboratory and field applications.

## 2. Fabrication of portable R.I. sensor

## 2.1. 3D-printed casing

In the development of our proposed smartphone-based R.I. sensor, we employ a 3D-printed casing to house the POFs. Fig. 1 illustrates the design of the 3D-printed casing for the proposed R.I. sensor. Fig. 1(a) highlights the precise dimensions and the 0.6 mm radius hole for the optical fibers, and Fig. 1(b) shows the front and back view of the casing for the POFs connector for the smartphone camera. The dimensions of the 3D-printed casing are meticulously determined to be 33.850 mm in height, 83.580 mm in width, and 53.814 mm in length, resulting in a total weight of just 32.88 g. These dimensions are selected to accommodate the optical fibers and the smartphone components while maintaining a lightweight and compact design. The precisely designed 0.6 mm radius hole in the connector ensures a secure fit around the fiber and complete encapsulation of the emitted light, minimizing potential sources of error and maximizing the accuracy of the R.I. measurements.

The choice of a 3D-printed casing is particularly advantageous because it allows for rapid prototyping and customization, enabling us to optimize the design according to the specific requirements of our R.I. sensor. The lightweight and compact design of the 3D-printed casing contributes to the overall portability and user-friendliness of the R.I. sensor. By combining the benefits of 3D printing technology with the precision of the designed connector, we have achieved a cost-effective

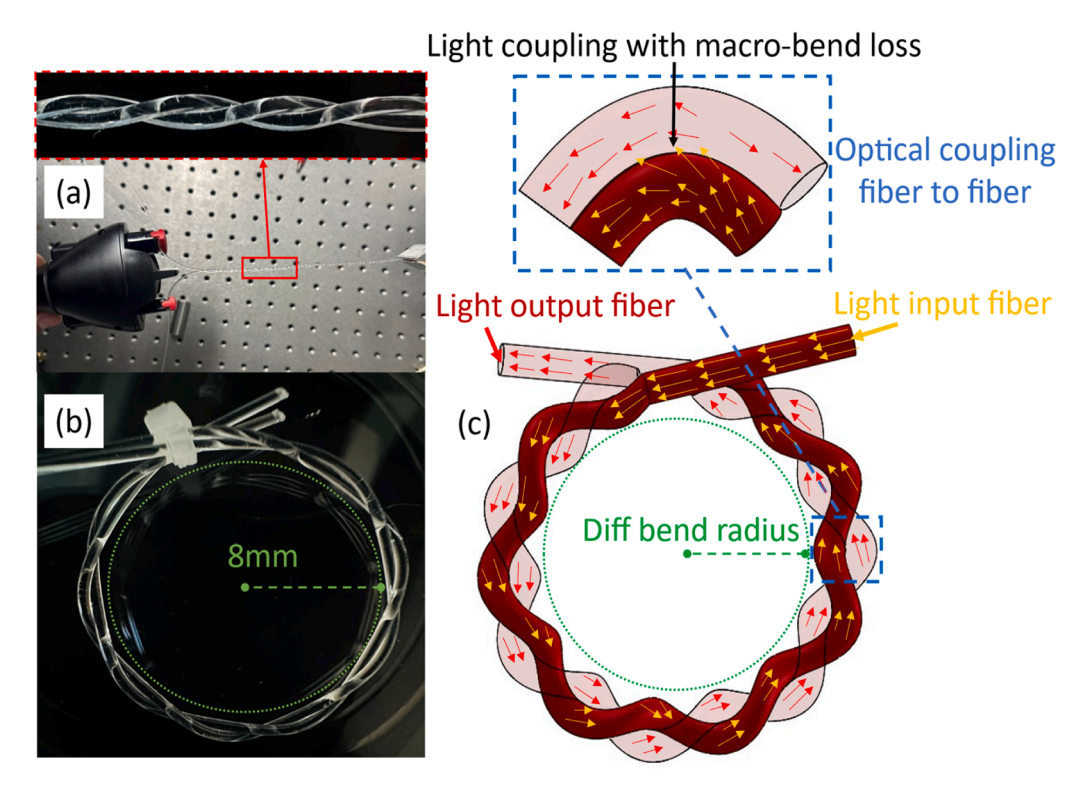


Fig. 2. Illustration of sensor fabrication. (a) twisting machine for uniform fiber twisting and structure without TMBOC, (b) TMBOC-based configuration with an 8 mm bend radius, (c) TMBOC technique for R.I. sensing and optical coupling.

and robust solution for R.I. sensing that can be easily deployed in various settings, ranging from laboratory experiments to field applications.

## 2.2. POF sensing using TMBOC

The proposed R.I. sensor design employs a method involving twisting structures using POFs. In this configuration, one fiber, designated as the primary fiber (PF), is responsible for propagating light and is connected to an LED source. The other fiber is referred to as coupled fiber (CF). The twisting fibers significantly influence the sensor's performance. To ensure uniform twisting and reliable sensor performance, we utilized a commercial hair-twisting machine, which maintained a consistent twist rate of 1 twist per centimeter, as shown in Fig. 2(a). This machine provided uniform twists, ensuring consistency in both the twist angle and pitch. Such uniformity was crucial for enhancing the repeatability and reliability of the sensor. The flexibility of the POF facilitates easy twisting without the need for additional temperature application, as twisting alone is sufficient to induce light coupling between the fibers. While the TMBOC fibers undergo a dual treatment: they are both twisted and subjected to macro-bending for efficient optical coupling, as shown in Fig. 2(b). This specific manipulation enables the fibers to become sensitive to changes in the R.I. of the surrounding medium.

When the R.I. of the surrounding medium varies, the light transmission pattern between the PF and CF also changes, thereby allowing for the measurement of the R.I. changes. Fig. 2(c) illustrates the method of with and without TMBOC, where PF and CF are optically coupled fiber-to-fiber, and demonstrates the power loss from PF due to external field-induced radiation and transmitted into the CF, which is a critical aspect of the sensor's operation.

This proposed technique for fabricating an R.I. sensor is based on the coupling power loss technique, which facilitates optical power coupling to detect changes in the R.I. This technique uses TMBOC to couple the radiated power from the PF and transmit it to the CF for R.I. measurement, as shown in Fig. 2(c). In this configuration, the PF generates bend loss, and the CF couples this loss, making the R.I. sensor more sensitive

to different refractive indices [38]. As light propagates through the twisted PF, some of it is lost due to the induced bend. This lost light is then coupled into the CF, whose efficiency in capturing this light is dependent on the R.I. of the surrounding medium. The closer the R.I. of the medium is to that of the fiber core, the more pronounced the coupling effect becomes. This property makes the sensor particularly sensitive to changes in the R.I. The sensor's ability to detect variations in R.I. is enhanced by the deliberate design of the coupling structure, which ensures that even small changes in the R.I. are captured by significant changes in the coupled power. This design feature is crucial for achieving high sensitivity in the sensor's response to R.I. fluctuations.

Although multimode optical fiber is sufficiently flexible to tolerate bending without significant loss, it also has certain drawbacks, which include signal latency distortions and scattering-induced light losses. To address these issues and evaluate the effects of macro-bending, several methods have been developed. To address these effects, various analytical and numerical methods such as ray tracing, beam propagation, finite element analysis, and numerical aperture techniques are employed. However, both beam propagation and finite element techniques have limitations in achieving exceptional accuracy due to their reliance on approximations and simplifications. Moreover, the numerical aperture method, while useful for initial estimations, lacks the capability for detailed optimization. In contrast, the ray-tracing method is advantageous because it requires lower computational complexity and provides greater precision compared to other methods. The sensitivity of the proposed R.I. sensor is based on the TMBOC technique, which can be optimized for specific requirements. The optical configuration for measuring the R.I. is founded on the TMBOC phenomenon, leveraging its unique characteristics to enhance the sensitivity and reliability of the

In the proposed setup, an input port  $P_{\rm in}$  is designated for the incoming light. The twisted PF radiates light from the light source, while the CF relies on the coupling of power loss for light propagation. The output power of the PF at the throughput port is denoted as  $P_0$ , and the output power of the CF is referred to as the coupled port  $P_{\rm couple}$  [39]:

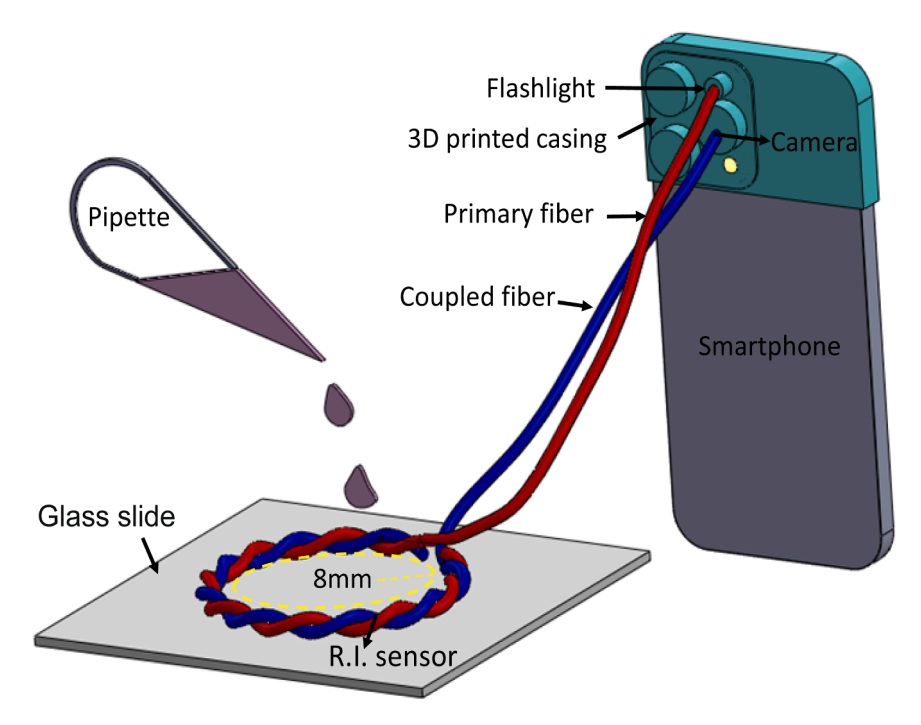


Fig. 3. Portable R.I. sensing illustration diagram.

$$P_{\text{couple}} = \frac{P_{\text{in}}}{1 + \left(\frac{a \cdot b \cdot n_{\text{eff}}}{\lambda}\right)^2} \tag{1}$$

where,  $P_{\rm in}$  is the input power, while a and b are sensitivity coefficients for bending and twisting and  $n_{\rm eff}$  is the effective R.I. and  $\lambda$  is the wavelength. The coupling coefficient K can be expressed as Eq. (2):

$$K = \frac{\sqrt{\frac{\delta \cdot \Delta n}{c^2 \cdot g}}}{1 - \left(\frac{n_{\text{clad}}}{n_{\text{core}}}\right)^2} \tag{2}$$

Here,  $\delta$  is a constant, while  $\Delta n$  is the R.I. difference. While c and g are constants related to fiber properties, and  $n_{\rm clad}$  and  $n_{\rm core}$  are the cladding and core refractive indices. Additionally, the coupling length L is defined in Eq. (3), where  $P_{\rm out}$  is the output coupled power form CF and n is the R. I. changes.

$$L = \frac{\pi \cdot P_{\text{out}}}{\sqrt{n \cdot K}} \tag{3}$$

## 2.3. Data analysis

As shown in Fig. 3, the smartphone-based sensing setup involves transmitting light and recording a video for intensity variation monitoring. The recorded video undergoes meticulous frame-by-frame analysis using MATLAB, a powerful tool for numerical computing. Each frame is first converted to grayscale using the 'rgb2gray' function, translating color information into a spectrum of gray values that directly correlate with brightness. Subsequently, the total light intensity for each frame is quantified by summing the gray values across all pixels, encapsulated by the following Eq. (4):

$$\textit{Light intensity} = \sum\nolimits_{i=1}^{M} \sum\nolimits_{j=1}^{N} \text{grayFrame}(i,j) \tag{4}$$

where M and N are the dimensions of the frame, as the resolution of video is  $1920 \times 1080$  as M and N set to 1920 and 1080, respectively. This systematic approach facilitates the computation of absolute intensities per frame, enabling seamless measurement through sequential

video analysis. For analytical purposes, the point at which the sensing area becomes fully dipped in the liquid is designated as the baseline or zero-level position, facilitating data normalization as:  $R = \frac{R_d}{R_0}$ . Where, R is the relative intensity, while  $R_0$  signifies the absolute intensity value at the (R.I.  $\approx$  1), and  $R_d$  denotes the sensor in liquid. Then the change in relative intensity  $\Delta R$  is expressed as:

$$\Delta R = \frac{(R_d - cR_0)}{R_0} \times 100\% \tag{5}$$

The correction factor c is applied to the baseline intensity  $R_0$ . The R.I. sensor sensitivity can be derived as follows:

$$S_{RL} = \frac{\Delta R}{\Delta n} \tag{6}$$

Here  $S_{R.I.}$  is the sensitivity, defined as the ratio of the change in relative intensity  $\Delta R$  to the corresponding change in R.I.  $\Delta n$ . To ensure measurement stability, the entire experimental setup, inclusive of the smartphone, remains stationary throughout the process. This precautionary measure eliminates the need for compensatory adjustments related to potential phone movement, streamlining the measurement protocol, and enhancing reliability.

## 3. Experimental setup

The smartphone-based R.I. sensing system leverages the capabilities of a smartphone, specifically an iPhone 14 Pro Max, to capture and process light-intensity data and monitor variations in light intensity. As shown in Fig. 3, the smartphone serves a dual purpose: generating light through its flashlight functionality and simultaneously capturing this light via the camera. The custom-designed 3D-printed casing, created using SolidWorks Pro software and printed on a Bambu Lab P1S 3D printer, plays a crucial role in ensuring the proper alignment and protection of the optical fibers and the smartphone components, as illustrated in Fig. 1(a-b). To facilitate these functions, the casing is attached to the smartphone, which is then mounted on a fixed stand. The PF is securely attached to the LED flashlight without any gaps, while the CF is positioned 0.5 mm away from the camera to allow for optimal focusing and light intensity measurement.

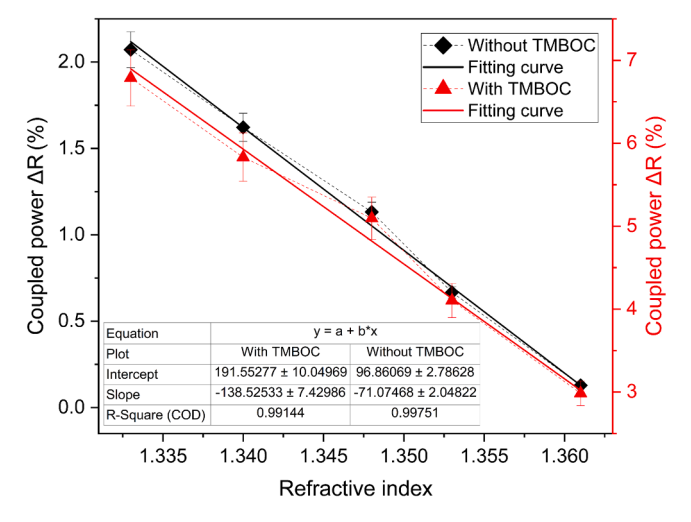


Fig. 4. Comparison of sensor sensitivity with and without TMBOC Effect.

For the R.I. sensor fabrication, we employ two individual pieces of uncoated POF. We specifically choose Mitsubishi Step Index SK-40 fiber for its elastic, soft, and flexible properties. The fiber core has a diameter of 980 μm, while the surrounding cladding layer is thicker than 20 μm, comprised of polymethyl methacrylate (PMMA) resin and a fluorinated polymer compound. The core R.I. is measured at 1.49. Importantly, the large core diameter and relatively thin cladding region contribute to significant bending-induced optical losses through side coupling effects. The CF is twisted around the PF to enable R.I. sensing. Upon completing the twisting, the initial and terminal sections were secured using nylon zip ties. The PF and the CF were subsequently guided through 3Dprinted casing, with the PF directly coupled to the smartphone's flashlight and the CF interfaced with the camera. In the configured system for R.I. sensing, the twisted coupling spanned 60 mm, resulting in a total fiber length of 1 m extending from the flashlight to the camera. The R.I. measurement employed the TMBOC, and the bend radius was 8 mm to achieve the maximum optical coupling fiber to fiber, as depicted in Fig. 2.

We prepared the sodium chloride solutions (NaCl) with varying concentrations and tested for their R.I. values using an Abbe refractometer. At a room temperature of  $25\,^{\circ}$ C, the respective liquid R.I. values were measured as 1.333, 1.340, 1.348, 1.353, and 1.361 for concentrations of  $0\,\%$ ,  $3.6\,\%$ ,  $7.2\,\%$ ,  $9.0\,\%$ , and  $12.6\,\%$ , respectively.

The StaCam app facilitates the video recording process by allowing users to customize video recording settings like ISO and shutter speed. These parameters are crucial for fine-tuning the camera's responsiveness to light, thereby ensuring optimal data accuracy. Adjusting ISO sensitivity is critical; however, excessively high settings can introduce unwanted noise, potentially compromising measurement integrity. Shutter speed calibration is equally important, as it controls light exposure and prevents intensity readings from becoming too low under noiseless ISO configurations. It is important to note that these settings are not static but require customization based on varying environmental conditions to ensure reliable and consistent performance.

## 4. Results and discussion

The performance of the R.I. sensor was meticulously evaluated to understand the impact of incorporating the TMBOC phenomena. Two configurations were compared: the TMBOC-based sensor and without TMBOC. The structure without TMBOC consisted of parallel twisted fibers without any deliberate macro-bending, relying solely on natural coupling between the fibers. As shown in Fig. 4, the sensor's response was analyzed both with and without the TMBOC technique, focusing on its sensitivity to various R.I. liquids. The R.I. sensor with TMBOC shows

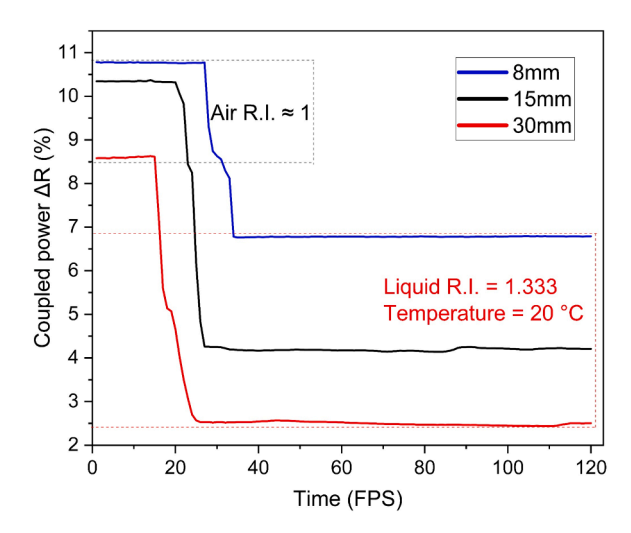


Fig. 5. Response of R.I. sensor at different bending radius and in same liquid with  ${\rm R.I.} = 1.333.$ 

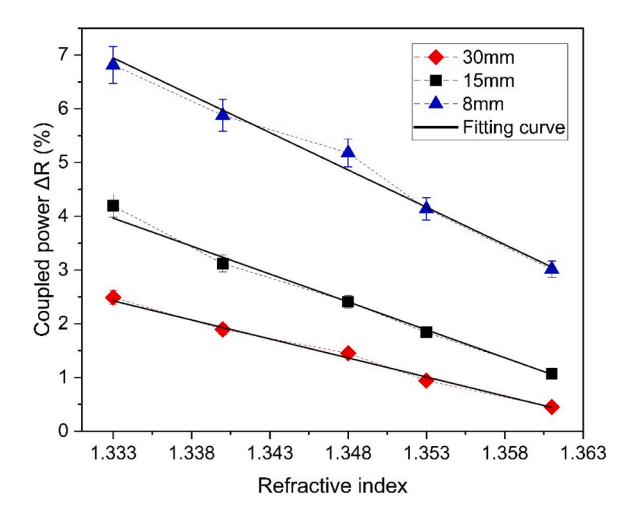


Fig. 6. Effect of bending radius on sensor performance.

a sensitivity of ( $S_{R.L}$  =137.2  $\pm$  2.3 %/RIU) compared to a sensitivity of ( $S_{R.L}$  =71.1  $\pm$  2.0 %/RIU) without TMBOC. The results reveal a marked improvement in the sensor's sensitivity when the TMBOC technique is employed.

The sensor with TMBOC exhibited a linear response with a correlation coefficient (R<sup>2</sup>) of 0.99144, indicating a coupling power loss with the change in the surrounding R.I. medium. The increase in sensitivity can be attributed to the TMBOC effect, which induces additional coupling power through the combined effects of twisting and macrobending. This enhanced coupling efficiency allows for more significant power loss when the fibers are exposed to liquids with varying R.I., improving the sensor's ability to detect minute changes in the R.I. This technique is particularly advantageous for detecting minute changes in the R.I., as the TMBOC enhanced sensor is more responsive compared to the sensor without TMBOC. The TMBOC technique is particularly advantageous for enhancing the sensor's responsiveness and overall performance compared to the configuration without TMBOC. These findings demonstrate the importance of combining twisting and macrobending to achieve optimal sensor performance. To further optimize the sensor's performance, the influence of different bending radii on the POF sensor was explored, as illustrated in Fig. 5.

The sensor's dynamic response to changes in the surrounding medium's R.I. was thoroughly examined, as shown in Fig. 5. In this experiment, the sensor was subjected to a transition from air R.I.  $\approx 1$  to a

**Table 1**The response of R.I. sensor at different bend radii.

| TMBOC diff<br>radii | Sensitivity<br>(%/RIU) | Y=ax+b                 | correlation<br>coefficient (R <sup>2</sup> ) |
|---------------------|------------------------|------------------------|--|
| 8                   | 139                    | -139.0083 + 192.24592  | 0.98897                                      |
| 15                  | 103                    | -103.86421 + 142.41604 | 0.99463                                      |
| 30                  | 70                     | -70.85051 + 96.87032   | 0.99365                                      |

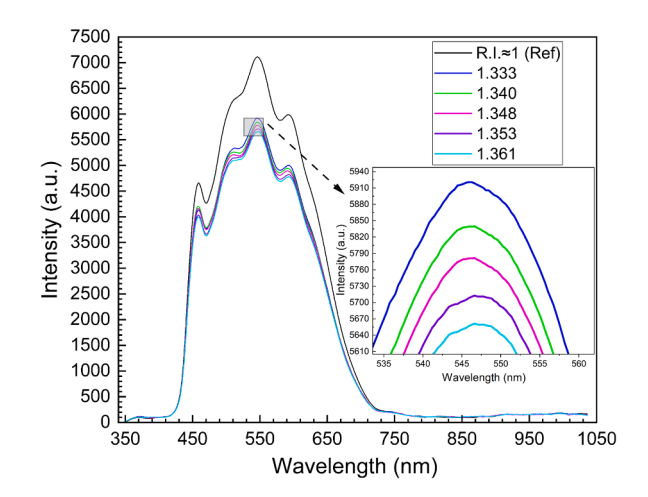


Fig. 7. Spectral response of the TMBOC-based 8 mm radius R.I. Sensor and impact of R.I. changes on the sensor's spectral response.

liquid with a R.I. of 1.333. The results clearly demonstrate the sensor's capability to detect rapid changes in R.I., as indicated by the significant decrease in coupled power loss immediately after immersion in the liquid. Notably, the sensor with an 8 mm bending radius outperformed the others, displaying the largest change in coupled power loss during the transition. This suggests that the sensor is highly sensitive to R.I. variations, making it suitable for real-time monitoring applications. The rapid stabilization of the sensor's response further highlights its potential for use in environments where quick and accurate R.I. measurements

To evaluate the effect on the R.I. sensor, we fabricated three different bending radii: 8 mm, 15 mm, and 30 mm. The analysis revealed that the sensor's sensitivity increases as the bending radius decreases, as depicted in Fig. 6. Specifically, the sensor with an 8 mm bending radius exhibited the highest sensitivity, with the largest coupled power loss observed across the range of refractive indices tested. This enhanced sensitivity can be explained by the macro-bend loss effect, which becomes more significant at smaller bending radii. When the bending radius is reduced, the core mode of the fiber undergoes transformation into a radiation mode, resulting in increased light leakage from the core into the cladding. This phenomenon enhances the interaction between the light field and the surrounding medium, thereby improving the sensor's ability to detect changes in the R.I. The experimental results align well with the theoretical model, where the radiated power R is given by,  $R = R_0 \times T$ , with  $R_0$  representing the initial power in the emitting fiber and T being the Fresnel transmission coefficient, the result are given in Table 1. The data confirms that smaller bending radii not only increase the radiation of the light field but also enhance the sensor's overall sensitivity, making it more effective for precise R.I.

To analyze the spectral behavior of the 8 mm radius sensor, the smartphone flashlight served as the light source, while the output was recorded using a spectrometer (Ocean Optics USB 2000+), which covers wavelengths from 340 to 1050 nm. The TMBOC configuration with an 8 mm bending radius was evaluated for its ability to detect R.I. variations by precisely measuring the fiber system's optical response to

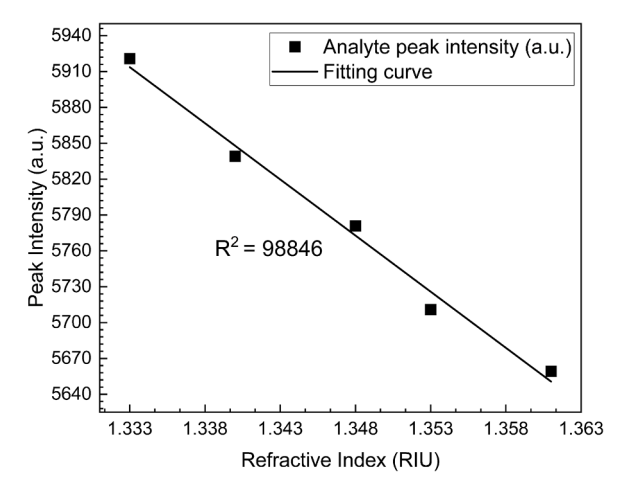
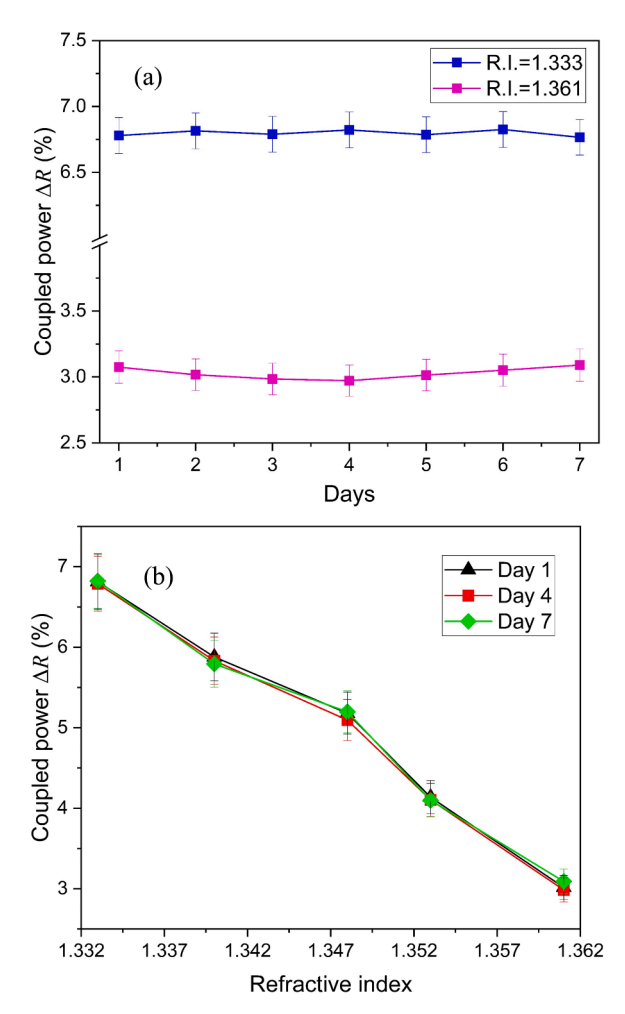


Fig. 8. Peak intensity response of the TMBOC-based 8 mm radius R.I. sensor.



**Fig. 9.** Repeatability and Stability of the smartphone-based R.I. sensor (a) showcases the repeatability and stability of the sensor over a period of seven days, and (b) demonstrates the sensor's consistent performance and suitability for long-term applications.

different R.I. mediums. Light was introduced into the PF, and the coupled power from the coupled fiber CF was captured by the spectrometer. Fig. 7 illustrates the spectral response of the TMBOC-based 8 mm radius R.I. sensor, showcasing the distinct transmission properties for different R.I. liquids.

Fig. 8 presents the peak intensity data extracted from the spectral

**Table 2**Comparison of proposed smartphone-based portable R.I. sensors with other POF proposed sensor in literature.

| Structure                      | Range (RIU)  | Resolution<br>(RIU)    | Sensitivity                     | Advantages  | Refs. |
|--------------------------------|--------------|------------------------|---------------------------------|---|-------|
| Tapering POF                   | 1.333-1.410  | Not mentioned          | 107 dB/RIU                      | High sensitivity, simple Fabrication.             | [27]  |
| Dual-tapering POF              | 1.33-1.41    | Not mentioned          | 950 μW/ RIU                     | Low cost, simple Fabrication.                     | [28]  |
| Side-polishing, bending        | 1.333-1.455  | $8.7 	imes 10^{-4}$    | 57 uW/ RIU                      | Low cost, hight sensitivity, stable.              | [29]  |
| Narrow groove coated gold film | 1.340-1.356  | Not mentioned          | 12.5 dB/ RIU (126 μW/           | Stable, high signal to-noise ratio, customizable. | [30]  |
| POF                            |              |                        | RIU)                            |   |       |
| In-line micro holes            | 1.33-1.42    | Not mentioned          | 13.4 dB/ RIU                    | Low cost, stable.                                 | [31]  |
| Drilling micro holes POF       | 1.333-1.475  | Not mentioned          | $-22.8\pm0.6$ %/RIU             | Portable, low cost.                               | [32]  |
| U-shaped notch POF             | 1.275-1.475, | Not mentioned          | $107.6 \pm 4.4  \%/\text{RIU},$ | Portable, customizable.                           | [33]  |
| Fiber-to-fiber Coupling POFs   | 1.333-1.361  | $1.065 \times 10^{-6}$ | $137.2 \pm 2.3~\%/\textrm{RIU}$ | Portable, easy fabrication, convenient, low cost, | This  |
|                                |              |                        |                                 | customizable                                      | work  |

response of the sensor, demonstrating the sensor's linear relationship with R.I. changes. The results show a high correlation coefficient (R² = 0.98846), consistent with the measurements obtained from the smartphone camera. These results confirm the strong correlation between the intensity variations and the R.I. changes. From these experiments, the resolution of the proposed TMBOC-based sensor with an 8 mm bending radius was calculated to be  $1.065 \times 10^{-6}$  RIU. This high resolution underscores the sensor's ability to detect extremely small changes in refractive index, making it suitable for high-precision applications.

The smartphone-based R.I. sensor must display exceptional repeatability and stability. To evaluate these characteristics, two supplementary experiments were conducted using the proposed setup. Fig. 9 illustrates the repeatability response of the sensor, showcasing good repeatability and consistent light intensity measurement for R.I.s of 1.333 and 1.361 over the course of seven days. As observed in the graph, the sensor's stability is demonstrated through overlapping data points representing the R.I. measurements on Days 1, 4, and 7, indicating minimal drift or degradation in performance. Overall, the sensor proves to be robust and reliable, making it well-suited for long-term applications.

Table 2 compares the proposed smartphone-based R.I. sensor with other methods found in the literature. Our approach stands out due to its simplicity, cost effectiveness, portability, and requiring only the smartphone's flashlight and camera for operation. The developed sensor maintains excellent consistency and reliability, with experimental results highlighting its stability as a portable sensor. The portable smartphone-based R.I. sensor's potential applications include diverse fields such as food quality control, medical diagnostics, and environmental monitoring.

### 5. Conclusion

The smartphone-based portable R.I. sensor fabricated using POF has demonstrated strong performance across various testing scenarios. The incorporation of the TMBOC effect significantly enhanced the sensor's sensitivity, allowing for more precise detection of R.I. changes. The analysis of different bending radii further confirmed that smaller radii, such as 8 mm, are optimal for maximizing sensitivity due to increased macro-bend loss and enhanced interaction between the light field and the surrounding medium. These findings have important practical implications for the design and application of POF-based R.I. sensors. The ability to detect minute changes in R.I. with high sensitivity and the capacity for real-time monitoring make this sensor highly versatile. It could be applied in fields such as biomedical sensing, environmental monitoring, and industrial process control, where accurate and rapid detection of refractive index changes is critical.

## CRediT authorship contribution statement

**Alathbah Moath:** Methodology. **Noor Laraib Unsa Noor:** Investigation, Formal analysis. **Ghaffar Abdul:** Writing – review & editing,

Methodology. Chen Chen: Writing – review & editing, Funding acquisition, Formal analysis. Haider Muhammad Saleh Urf Kumail: Writing – original draft, Methodology. Arman MD. Bipu: Investigation. Hussain Sadam: Validation, Investigation. Liu Min: Investigation, Funding acquisition.

## **Declaration of Competing Interest**

No, I declare that the authors have no competing interests as defined by Nature Research, or other interests that might be perceived to influence the results and/or discussion reported in this paper.

## Acknowledgment

This research was supported by the National Natural Science Foundation of China under Grant 61901065, and in part by the Fundamental Research Funds for the Central Universities under Grant 2024CDJXY020.

Informed Consent Statement

Not applicable.

## Author Contributions Statement

Formal analysis, Chen Chen and Laraib Unsa Noor; Funding acquisition, Chen Chen and Min Liu; Investigation, Min Liu, Sadam Hussain, MD. Bipu Arman and Laraib Unsa Noor; Methodology, Muhammad Saleh Urf Kumail Haider, Moath Alathbah and Abdul Ghaffar; Validation and Review, Chen Chen, Abdul Ghaffar, and Sadam Hussain; Writing – original draft Muhammad Saleh Urf Kumail Haider.

## Data availability

Data will be made available on request.

## References

- Y. Xu, et al., "Optical refractive index sensors with plasmonic and photonic structures: promising and inconvenient truth, Adv. Opt. Mater. 7 (9) (2019) 1801433. https://doi.org/10.1002/adom.201801433.
- [2] R. Khan, B. Gul, S. Khan, H. Nisar, I. Ahmad, "Refractive index of biological tissues: review, measurement techniques, and applications, Photo Photo Ther. 33 (Mar 2021) 102192, https://doi.org/10.1016/j.pdpdt.2021.102192.
  [3] M. Elsherif, et al., "Optical fiber sensors: working principle, applications, and
- [3] M. Elsherif, et al., "Optical fiber sensors: working principle, applications, and limitations, Adv. Photonics Res. 3 (11) (2022) 2100371, https://doi.org/10.1002/ adpr.202100371.
- [4] C. Teng et al., "Intensity-Modulated Polymer Optical Fiber-Based Refractive Index Sensor: A Review," Sensors, vol. 22, no. 1, doi: 10.3390/s22010081.
- [5] M.G. López Aveiga, M.D.F. Ramos, V.M. Núnez, L.F.C. Vallvey, A.G. Casado, A. L. Medina Castillo, "Portable fiber-optic sensor for simple, fast, cost-effective, and environmentally friendly quantification of total acidity in real-world applications, Sens. Actuators B: Chem. 417 (2024) 136214, https://doi.org/10.1016/j.snb.2024.136214.

- [6] X. Zhang, C. Wang, T. Zheng, H. Wu, Q. Wu, and Y. Wang, "Wearable Optical Fiber Sensors in Medical Monitoring Applications: A Review," Sensors, vol. 23, no. 15, doi: 10.3390/s23156671.
- [7] R. Jha, P. Mishra, S. Kumar, "Advancements in optical fiber-based wearable sensors for smart health monitoring, Biosens. Bioelectron. 254 (Jun 15 2024) 116232, https://doi.org/10.1016/j.bios.2024.116232.
- [8] S. Rasheed, T. Kanwal, N. Ahmad, B. Fatima, M. Najam-ul-Haq, D. Hussain, "Advances and challenges in portable optical biosensors for onsite detection and point-of-care diagnostics, TrAC Trends Anal. Chem. 173 (2024) 117640, https:// doi.org/10.1016/j.trac.2024.117640.
- [9] S. Hassani and U. Dackermann, "A Systematic Review of Advanced Sensor Technologies for Non-Destructive Testing and Structural Health Monitoring," Sensors, vol. 23, no. 4, doi: 10.3390/s23042204.
- [10] B. Yang, B. Yang, J. Zhang, Y. Yin, Y. Niu, and M. Ding, "A Sensing Peak Identification Method for Fiber Extrinsic Fabry–Perot Interferometric Refractive Index Sensing," Sensors, vol. 19, no. 1, doi: 10.3390/s19010096.
- [11] C. Zhou, Q. Zhou, C. He, J. Tian, Y. Sun, Y. Yao, "Fiber optic sensor for simultaneous measurement of refractive index and temperature based on internaland- external-cavity fabry-pérot interferometer configuration, IEEE Sens. J. 21 (8) (2021) 9877–9884, https://doi.org/10.1109/jsen.2021.3059021.
- [12] Z. Wang, C. Yao, Y. Zhang, Y. Su, "Compact silicon three-mode multiplexer by refractive-index manipulation on a multi-mode interferometer, Opt. Express 29 (9) (Apr 26 2021) 13899–13907, https://doi.org/10.1364/OE.423973.
- [13] C. Peng et al., "Optical Waveguide Refractive Index Sensor for Biochemical Sensing," Applied Sciences, vol. 13, no. 6, doi: 10.3390/app13063829.
- [14] H.C.A.S.G. Vasconcelos, J.M.M.M. d Almeida, C.M.T. Saraiva, P.A. d S. Jorge, L.C. C. Coelho, Mach–Zehnder interferometers based on long period fiber grating coated with titanium dioxide for refractive index sensing, J. Light. Technol. 37 (18) (2019/09) 4584–4589. (https://opg.optica.org/jlt/abstract.cfm?URI=jlt-37-18-4584)
- [15] X. Lei, X. Dong, T. Sun, K.T.V. Grattan, "Ultrasensitive refractive index sensor based on mach–zehnder interferometer and a 40μm fiber, J. Light. Technol. 39 (17) (2021) 5625–5633. (https://opg.optica.org/jlt/abstract.cfm?URI=jlt-39-17-5625).
- [16] J. Hovik, M. Yadav, J. Wook Noh, A. Aksnes, "Waveguide asymmetric long-period grating couplers as refractive index sensors, Opt. Express 28 (16) (Aug 3 2020) 23936–23949, https://doi.org/10.1364/OE.397561.
- [17] Q. Ling, Z. Gu, X. Jiang, K. Gao, "Design of long period fiber grating surrounding refractive index sensor based on mode transition near phase-matching turning point, Opt. Commun. 439 (2019) 187–192, https://doi.org/10.1016/j. optcom.2019.01.060.
- [18] P. Tian, et al., "Refractive index sensor based on fiber bragg grating in hollow suspended-core fiber, IEEE Sens. J. 19 (24) (2019) 11961–11964, https://doi.org/ 10.1109/isen.2019.2938786.
- [19] H. Yang, Y. Li, X. Li, "Intensity-modulated refractive index sensor based on the side modes of fiber Bragg grating, Opt. Commun. 505 (2022) 127319, https://doi.org/ 10.1016/j.optcom.2021.127319.
- [20] P. Xue, F. Yu, Y. Cao, J. Zheng, "Refractive index sensing based on a long period grating imprinted on a multimode plastic optical fiber, IEEE Sens. J. 19 (17) (2019) 7434–7439, https://doi.org/10.1109/jsen.2019.2915361.
- [21] J.J. Patil, Y.H. Patil, A. Ghosh Comprehensive and Analytical Review on Optical Fiber Refractive Index Sensor," in 2020 4th International Conference on Trends in Electronics and Informatics (ICOEI)(48184), 15-17 June 2020 2020, pp. 169-175, doi: 10.1109/ICOEI48184.2020.9142916..
- [22] J. Shi, et al., "A high-resolution liquid-level sensor based on fabry-perot interferometer with fiber laser intracavity sensing, IEEE Sens. J. 23 (15) (2023) 16938–16943, https://doi.org/10.1109/jsen.2023.3288223.
- [23] F. Ye, C. Tian, C. Ma, Z.F. Zhang, "Fiber optic sensors based on circular and elliptical polymer optical fiber for measuring refractive index of liquids, Opt. Fiber Technol. 68 (2022) 102812, https://doi.org/10.1016/j.yofte.2021.102812.
- [24] P. Roriz, A. Ramos, J.L. Santos, J.A. Simões, "Fiber optic intensity-modulated sensors: a review in biomechanics, Photon. Sens. 2 (4) (2012) 315–330, https:// doi.org/10.1007/s13320-012-0090-3.
- [25] J.J. Patil, Y.H. Patil, A. Ghosh, "Fiber optics refractive index sensor based on intensity modulation, 4th Int. Conf. Electron., Commun. Aerosp. Technol. (ICECA) (2020) 623–628, https://doi.org/10.1109/ICECA49313.2020.9297477.
- [26] X. Hu, C.-F.J. Pun, H.-Y. Tam, P. Mégret, C. Caucheteur, "Tilted Bragg gratings in step-index polymer optical fiber, Opt. Lett. 39 (24) (2014) 6835–6838, https://doi. org/10.1364/OL.39.006835
- [27] H. Ujihara, N. Hayashi, K. Minakawa, M. Tabaru, Y. Mizuno, K. Nakamura, "Polymer optical fiber tapering without the use of external heat source and its application to refractive index sensing, Appl. Phys. Express 8 (7) (2015) 072501, https://doi.org/10.7567/apex.8.072501.
- [28] F. De-Jun, L. Guan-Xiu, L. Xi-Lu, J. Ming-Shun, S. Qing-Mei, "Refractive index sensor based on plastic optical fiber with tapered structure, Appl. Opt. 53 (10) (2014) 2007–2011, https://doi.org/10.1364/AO.53.002007.
- [29] F. De-Jun, Z. Mao-Sen, G. Liu, L. Xi-Lu, J. Dong-Fang, "D-shaped plastic optical fiber sensor for testing refractive index,", IEEE Sens. J. 14 (5) (2014) 1673–1676, https://doi.org/10.1109/jsen.2014.2301911.
- [30] Y. Hu, Y. Hou, A. Ghaffar, W. Liu, "A narrow groove structure based plasmonic refractive index sensor, IEEE Access 8 (2020) 97289–97295, https://doi.org/ 10.1109/access.2020.2993707.
- [31] J.-D. Shin, J. Park, "Plastic optical fiber refractive index sensor employing an inline submillimeter hole, IEEE Photonics Technol. Lett. 25 (19) (2013) 1882–1884, https://doi.org/10.1109/lpt.2013.2278973.

- [32] Y. Ye, C. Zhao, Z. Wang, C. Teng, C. Marques, R. Min, "Portable multihole plastic optical fiber sensor for liquid-level and refractive index monitoring, IEEE Sens. J. 23 (3) (2023) 2161–2168, https://doi.org/10.1109/jsen.2022.3228224.
- [33] C. Zhao, Y. Ye, Z. Wang, C. Teng, R. Min, "Notch POF integrated with smartphone for liquid level and refractive index monitoring, Opt. Laser Technol. 167 (2023) 109751, https://doi.org/10.1016/j.optlastec.2023.109751.
- [34] C. Yang, et al., "Portable optical fiber biosensors integrated with smartphone: technologies, applications, and challenges [Invited, Biomed. Opt. Express 15 (3) (Mar 1 2024) 1630–1650, https://doi.org/10.1364/BOE.517534.
- [35] J. Huang *et al.*, "Smartphone-Based Optical Fiber Fluorescence Temperature Sensor," Sensors, vol. 22, no. 24, doi: 10.3390/s22249605.
- [36] J.D. Malone, I. Hussain, A.K. Bowden, "SmartOCT: smartphone-integrated optical coherence tomography, Biomed. Opt. Express 14 (7) (Jul 1 2023) 3138–3151, https://doi.org/10.1364/BOE.492439.
- [37] R. Kuang, et al., "Low-cost plastic optical fiber integrated with smartphone for human physiological monitoring, Opt. Fiber Technol. 71 (2022) 102947, https://doi.org/10.1016/j.yofte.2022.102947.
- [38] A.K. Agarwal, "Review of optical fiber couplers, Fiber Integr. Opt. 6 (1) (1987) 27–53.
- [39] A.W. Snyder, "Coupled-mode theory for optical fibers, JOSA 62 (11) (1972) 1267–1277.



Muhammad Saleh Urf Kumail Haider received the B.S. degree in Electronics Engineering from the University of Sindh, Jamshoro, Pakistan, in 2022. He is currently pursuing the M. Eng. degree with the School of Microelectronics and Communication Engineering, Chongqing University, Chongqing, China. His research interests include optical fiber sensing, smartphone-based sensors, artificial intelligence integration in sensor systems, and portable, real time monitoring solutions.



Chen Chen received the B.S. and M.Eng. degrees from the University of Electronic Science and Technology of China, Chengdu, China, in 2010 and 2013,respectively, and the Ph.D. degree from Nanyang Technological University, Singapore, in 2017. He was a Post-Doctoral Researcher with the School of Electrical and Electronic Engineering, Nanyang Technological University, from 2017 to 2019. He is currently a Professor with the School of Microelectronics and Communication Engineering, Chongqing University, Chongqing, China. His research interests include optical wireless communication and optical sensing.



Abdul Ghaffar was born in 1991 in Pakistan. He did his bachelor from QUEST Nawabshah master from Indus University, and Ph.D degree from the North University of China in the field instrumentation technology. Previously, He was the Lecturer in Indus University Karachi of Pakistan. He did post-doc from Wuhan Institute of rock and soil mechanics, University of Chinese Academy of Sciences in 2023. Currently, he is working in Quzhou University as an assistant professor from 2023. He has published more than 35 SCI papers in various reputed journals. His research directions are Sensor's technology, optical fiber sensor, Polymer optical fiber, distributed sensor and displacement sensor.



Laraib Unsa Noor received her B.S. degree in Electronics Engineering from the University of Sindh, Jamshoro, Pakistan, in 2022. She is currently pursuing an M.Eng. degree at the College of Mechanical and Vehicle Engineering, Chongqing University, Chongqing, China. Her research interests include fast charging strategies for electric vehicles (EVs) and optical fiber sensing for temperature and pH sensors.



Min Liu received the B.S. degree in electromagnetic measurement and instrument from Chongqing University, Chongqing, China, in 1997 and the Ph.D. degree from Nanyang Technology University, Singapore, in 2004.,She is a Professor in college of communication engineering, Chongqing University. Her research interests include optical fiber communication and fiber sensors. She is a Member of the Optical Society of America. She has published more than 20 papers in the international journals, including IEEE Journal of Quantum Electronics, IEEE Photonics Technology Letters, Optics Express, Applied Physics B, and Optics Communications.



**Bipu Arman** completed his B.S. degree in Electronics Information Engineering at China West Normal University, Sichuan, China, in 2023. He is currently enrolled in the M.Eng. program at the School of Optoelectronic Engineering, Chongqing University, Chongqing, China. His research focuses on bio-sensing, microcavities, and biomechanics.



Sadam Hussain is an Assistant Professor at Quzhou Univeristy since 2022. He obtained his PhD and Master's degree from School of Energy and Power Engineering, Xi'an Jiaotong University in 2022 and 2018. He obtained his Bachelor's degree from department of Energy and Environmental Engineering, Quaide-Awam University of Engineering Science and Technology (Pakistan) in 2015. His research interests mainly cover the optical fiber sensor, polymer fiber, robotics, heat transfer and film cooling in gas turbine blade.

Moath Alathbah received the Ph.D. degree from Cardiff University, U.K. He is currently an Assistant Professor with King Saud University, Saudi Arabia. His research interests include the development of photoelectronic, integrated electronic active and passive discrete devices, the design, fabrication, and characterization of MMIC, RF and THz components, smart antennas, microstrip antennas, microwave filters, meta-materials, 5 G antennas, MIMO antennas miniaturized multiband/wideband antennas, and microwave/millimeter components using micro and nanotechnology.